2021 43rd Annual International Conference of the
IEEE Engineering in Medicine & Biology Society (EMBC)
Oct 31 - Nov 4, 2021. Virtual Conference

MRI Knee Domain Translation for Unsupervised Segmentation By CycleGAN (data from Osteoarthritis initiative (OAI))

Banafshe Felfeliyan [1], Abhilash Hareendranathan [2] , Gregor Kuntze [1], Jacob Jaremko[2] and Janet Ronsky[1]

***Abstract*— Accurate quantification of bone and cartilage features is the key to efficient management of knee osteoarthritis (OA). Bone and cartilage tissues can be accurately segmented from magnetic resonance imaging (MRI) data using supervised Deep Learning (DL) methods. DL training is commonly conducted using large datasets with expert-labeled annotations. DL models perform better if distributions of testing data (target domains) are close to those of training data (source domains). However, in practice, data distributions of images from different MRI scanners and sequences are different and DL models need to re-trained on each dataset separately. We propose a domain adaptation (DA) framework using the CycleGAN model for MRI translation that would aid in unsupervised MRI data segmentation. We have validated our pipeline on five scans from the Osteoarthritis Initiative (OAI) dataset. Using this pipeline, we translated TSE Fat Suppressed MRI sequences to pseudo-DESS images. An improved MaskRCNN (IMaskRCNN) instance segmentation network trained on DESS was used to segment cartilage and femoral head regions in TSE Fat Suppressed sequences. Segmentations of the I-MaskRCNN correlated well with approximated manual segmentation obtained from nearest DESS slices (DICE = 0.76) without the need for retraining. We anticipate this technique will aid in automatic unsupervised assessment of knee MRI using commonly acquired MRI sequences and save experts' time that would otherwise be required for manual segmentation.**

***Clinical relevance*— This technique paves the way to automatically convert one MRI sequence to its equivalent as if acquired by a different protocol or different magnet, facilitating robust, hardware-independent automated analysis. For example, routine clinically acquired knee MRI could be converted to high-resolution high-contrast images suitable for automated detection of cartilage defects.**

I. INTRODUCTION

Knee osteoarthritis (OA) significantly reduces quality of life and creates a substantial financial healthcare burden. There is a growing need for techniques that accurately quantify and track the extent of tissue damage and identify potential targets for treatment. Effective long-term OA follow-up is often hampered by a lack of accurate reproducible biomarkers. MRI can be used to study structural change in OA based on cartilage thickness, which has been used to predict knee replacement [1] and validate alternative intervention [2]. Regional differences in cartilage thickness have also been correlated with joint space narrowing (JSN) [3] which is a well-established radiographic marker of OA progression. Changes in cartilage thickness and volume between subregions of the knee have further been used to establish a timeline for survival rate [4].

Automatic or semi-automatic measurements are suited for longitudinal assessment of knee MRI as it reduces the possible variability between readers and saves time. Segmentation of knee tissue from MRI is a key to measuring cartilage thickness. Deep Learning (DL) based techniques using Convolutional Neural Networks (CNN) have shown great success in knee and hip tissue and pathology segmentation [5]–[10]. These techniques use supervised learning and are trained on large datasets with ground truth. However, the accuracy of DL models trained on one dataset (source dataset) drops when it is tested on a new dataset collected (target dataset) in a dissimilar imaging circumstance. Generally, source and target datasets have different data distribution due to the domain shift across different vendors, data collection centers, image acquisition protocols and sequences. Each dataset with a specific imaging protocol, modality, or vendor can be considered as a point on a high-dimensional non-linear manifold with significant differences in their statistical distribution [11]. Retraining these models requires expert-labeled annotations for each dataset and human readers with medical expertise, which are time-consuming and expensive. Therefore, the need for generalizable DL models that perform well on unseen data or data without annotations is increasingly gaining recognition [11]–[13]. Consequently, Unsupervised Domain Adaptation (UDA) and domain generation techniques that enable an existing model to adapt to multiple datasets have generated research interest [11]. These approaches aim to reduce data distribution differences between source and target data when annotation is not available.

The popular domain adaptation technique of image adaptation aligns the appearance of an image between two domains by pixel-to-pixel transformation [14]. In natural images, such pixel-to-pixel transformation can be obtained by image translation using Generative Adversarial Networks (GAN) [15]. Cycle consistent GAN (CycleGAN) [16] is a suitable candidate for medical images pixel-to-pixel domain adaptation [12], [13] as they enforce a reverse mapping between the source image and the generated image which reduces the chance of generating images that are anatomically improbable. CycleGANs have been used in MRI for compressed sensing, improving the quality of segmentation and domain adaptation [17].

In this paper we propose to translate unpaired MRI data

[1]Felfeliyan, Kuntze, and Ronsky are with the University of Calgary, 2500 University DR, Calgary, AB, T2N 1N4, Canada banafshe.felfeliyan@ucalgary.ca

[2]Hareendranathan and Jaremko are with the University of Alberta, 2A2.41 WMC, 8440 – 112 St. NW, Edmonton, AB, Canada hareendr@ualberta.ca

from the source domain (COR IW 2D TSE Fat Suppressed MRI) to the target domain (Sagittal 3D DESS WE) and pass the generated pseudo target domain images to the segmentation algorithm. As the TSE Fat Suppressed is a common clinical sequence and with availability of the large labeled datasets like those of the Osteoarthritis Initiative (OAI) we can translate the clinical images to research sequences to extract meaningful information from clinical images. We accomplished this goal using the CycleGAN model for image translation, which reinforces the reverse mapping between two MRI modalities. Further, to make the network aware of context of interest, we passed DESS segmentation labels to the network. Bone and cartilage tissues in the source were segmented using an I-MaskRCNN [9], [18] model trained on labeled image from the target.

II. Proposed Methodology

The I-MaskRCNN instance segmentation network was trained to identify cartilage tissue in DESS MRI slices. The CycleGAN was then used to segment 2D TSE Fat Suppressed MRI data without retraining (fig. 1). The CycleGAN architecture and I-MaskRCNN are explained in the following sections.

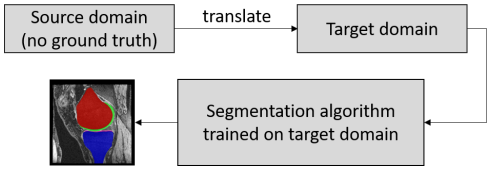

Fig. 1. Segmentation using domain translation pipeline.

A. Data Preparation

The sagittal DESS MRI data were re-sliced into the coronal view. Furthermore, to have the same field of view (FOV) and matrix size, the re-sliced images were interpolated, and zero padding was incorporated. Additionally, the bone and cartilage segmentation labels were added to the images as the third channel. Adding bone and cartilage labels gives additional context aware information to the network.

B. CycleGAN

CycleGAN improves upon the GAN architecture by introducing two generators for mapping from source-to-target (in this paper $G_{TSE \rightarrow DESS}$ (fig. 2) and from target-to-source (in this paper $G_{DESS \rightarrow TSE}$) and two discriminators (D_{TSE} and D_{DESS} (fig. 2) for adversarial learning [16]. The latter is an inverse mapping that ensures similarly with the original image and is represented as the cycle consistency loss:

$$L_{cycle}(G_x, G_y) = E_{x \sim pdata(x)}[\|x - G_x(G_y(x)\|_1] + E_{y \sim pdata(y)}[\|y - G_y(G_x(y)\|_1]. \quad (1)$$

Furthermore, the identity loss is deployed for the time that real samples of a given domain are provided as input to the generator, to regularize the generator to be close to an identity mapping [16]:

$$L_{identity}(G_x, G_y) = E_{y \sim pdata(y)}[\|G_y(y) - y\|_1] + E_{x \sim pdata(x)}[\|G_x(x) - x\|_1] \quad (2)$$

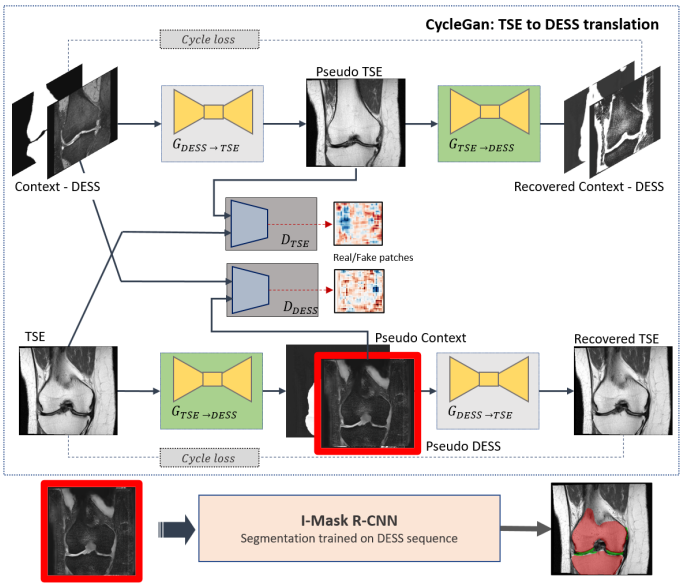

Fig. 2. (I) Overview of the CycleGAN model Using the 2D TSE Fat suppressed MRI slice the CycleGAN generates a pseudo-DESS image which is segmented by the I-MaskRCNN.

The adversarial loss is applied to both mapping functions.The adversarial loss for the mapping function $G : X \rightarrow Y$ and its corresponding discriminator D_y would be:

$$L_{GAN}(G, D_y, X, Y) = E_{y \sim pdata(y)}[logD_Y(y)] + E_{x \sim pdata(x)}[log(1 - D_Y(G(x))]. \quad (3)$$

C. I-Mask RCNN

The MaskR-CNN instance segmentation network model [19] is constructed from a backbone which is responsible for feature extraction, a region proposal network responsible for extracting the bounding box around the region of interest, and two heads: one for mask segmentation, and the other for classifying the extracted bounding boxes. This model gave highly accurate instance segmentation of objects on various natural image datasets. I-Mask RCNN is a modified version of the original Mask RCNN that improves the segmentation accuracy around object boundaries by adding a skip connection and adding an encoder layer to the mask segmentation head [9], [18]. This feature is particularly useful in detecting faint boundaries between anatomical structures seen in medical images. The pseudo–COR-DESS MRI slices generated using the CycleGAN were forwarded to the I-Mask RCNN for the segmentation of bone and cartilage.

D. Training

The CycleGAN was trained on 8000 MRI slices of the clinical TSE Fat Suppressed sequences (the source domain) and 12000 of MRI slices of higher quality DESS sequences (the target domain). The Mask-RCNN network was trained on 300 DESS sequence MRI (resliced to COR view) scans.

III. Data

Data from the National Institutes of Health (NIH) sponsored multicenter Osteoarthritis Initiative (OAI) dataset was used to validate our approach. OAI includes MRI data

obtained from 4706 subjects aged between 45 and 79 years. Knee imaging was performed using 3.0 Tesla MRI scanners. COR IW TSE Fat Suppressed sequence is one of the OAI data protocols for highlighting medial cruciate ligaments and marginal femoral and tibial osteophytes [20]. Sagittal 3D DESS provides good cartilage discrimination. A high number of segmentation labels are available through the OAI-ZIB dataset [21].

A. Validation

The results of the image translation were validated on 2 metrics: 1. Image similarity of the generated image with the nearest DESS image slice from the same patient using the cosine similarity (CS) measure, and 2. Accuracy of segmentation of a trained I-MaskRCNN network on pseudo-DESS images generated using CycleGAN using the dice score (DS). These measures are defined below as:

$$CS = \frac{I_{psedudo_{DESS}}.I_{DESS}}{\|I_{psedudo_{DESS}}\|.\|I_{DESS}\|} \tag{4}$$

$$DS = \frac{2 \times |P \bigcap GT|}{|P| + |GT|} \tag{5}$$

where $I_{pseudo-DESS}$, I_{DESS}, P and GT represent the pseudo-DESS image, original DESS image, predicted mask and ground truth segmentation, respectively.

IV. Results

The trained CycleGAN on PDFS and DESS images is validated on 125 images from five patients randomly sampled from the remaining images in the OAI dataset.

A. Image Similarity

CycleGAN was able to generate pseudo-DESS images that closely resembled the slices in the DESS image (fig. 3). Pseudo-DESS and original DESS images (i.e. anterior, mid and posterior knee joint segments) of the same individual were qualitatively compared. For each TSE image slice, the closest DESS MRI slice (based on the position information in the DICOM header) was selected manually and the cosine similarity of this image with the pseudo-DESS image was calculated. The pseudo-DESS images showed high cosine similarity of 0.86 over the test dataset (Table I).

B. Accuracy of Segmentation

The trained I-MaskRCNN achieved dice score of 0.95 on DESS images and then tested on: 1. Original TSE slices (with no image translation), and 2. pseudo-DESS images generated by the CycleGAN. The I-Mask R-CNN was almost unable to generate segmentation on TSE data, there results were inaccurate and gave a very low dice score of 0.1. By changing the data distribution the segmentation on pseudo-DESS showed high agreement with expert segmentations (fig. 4).

Difference in segmentation accuracy was statistically significant between pseudo-DESS (dice score = 0.73) vs original TSE (dice score = 0.1) images p-value < 0.05 (Table I).

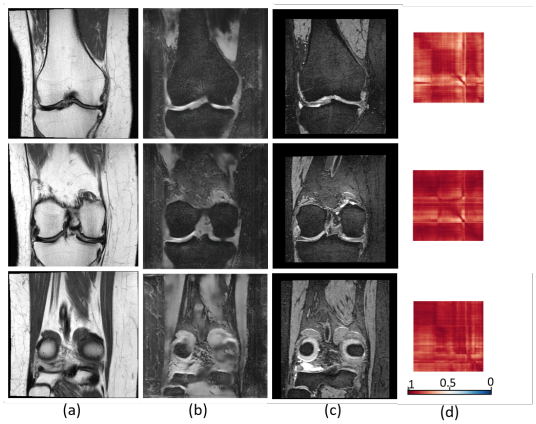

Fig. 3. Image translation results. (a) TSE sequence; (b) CycleGAN' s result pseudo-DESS; (c) original DESS (nearest slice to pseudo DESS). (d) cosine similarity between pseudo DESS and nearest real DESS slice (1(red)= high similarity, 0 (blue) = low similarity).

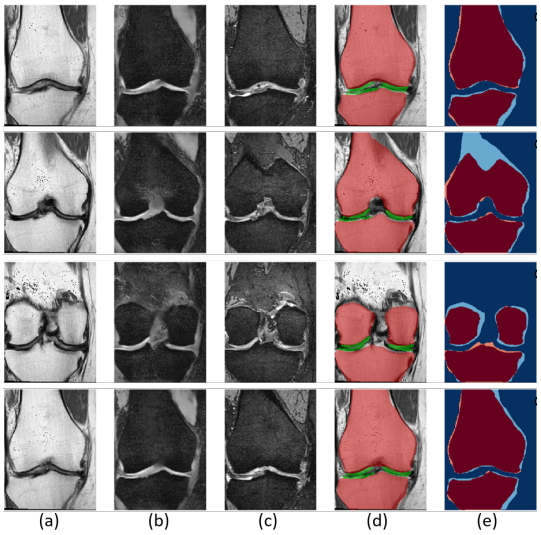

Fig. 4. CycleGAN pipeline results. (a) TSE; (b) pseudo DESS; (c) nearest real DESS slice; (d) segmentation overlayed on TSE; (e) difference between nearest DESS slice label and segmentation result (red: overlap, blue= pseudo DESS, orange= DESS label).

V. Discussion

In this paper, we developed a technique to translate between two different MRI sequences - 2D PDFS and 3D DESS - which were extracted from the OAI data. These sequences were chosen because their perceptual differences are great and the domain shift phenomenon between them is readily observable and due to shortage of label for retraining networks on clinical sequences.

CycleGANs have been used for image translation in similar applications in natural and medical images. This work is one of the first attempts for image-to-image translation between different knee MRI sequences using CycleGAN.

Since the CycleGAN performs unpaired translation, no correspondence was required between the images during training. On a set of five scans, pseudo-DESS images generated using CycleGAN showed more similarity (cosine similarity 0.86 vs 0.8)) with the closest slice in the actual DESS sequence than the TSE sequance. As an indirect measure of the quality of image translation, we also exam-

TABLE I
COSINE SIMILARITY (CS) AND DICE SCORE

	CS	DS I-MaskRCNN
Original TSE	0.80	0.13
Pseudo-DESS (CycleGAN)	0.86	0.73

ined the performance of a trained I-MaskRCNN instance segmentation network on original PDFS (with no image translation) and pseudo-DESS data from the CycleGAN. The trained I-MaskRCNN gave acceptable segmentations on pseudo-DESS data generated from CycleGAN (dice score 0.73). Segmentation images generated from pseudo-DESS showed high agreement with ground truth segmentation upon visual inspection and were suitable for measuring cartilage thickness which is an important OA biomarker.

The limitation of our study first is that our MRI is acquired using high resolution 3T MRI scanners that might not be available in all clinics. As an extension of this work, we plan to adapt the CycleGAN approach to translate between low quality 1.5 T MR images to pseudo-3T MR images. Along similar lines, our approach would also be extended to similar applications in hip MRI where lower quality images can be enhanced for identifying OA biomarkers like effusion. Second, CycleGAN potentially generates spurious artefacts in the pseudo-DESS image. This limitation is addressed in part by improving adding segmentation label to make the network context aware. However, in some anterior and posterior slices we observed that both models generated spurious bright artefacts and dark patches. Another limitation pertains to the need for large dataset for training CycleGANs. Unlike natural images where large numbers of labeled images are available, labeled medical image data (and MRI in particular) is scarce. Future extensions of this study would aim to address this limitation by collecting large numbers of MRI data prospectively and incorporating retrospectively collected MRI images from multiple centers.

VI. CONCLUSION

We proposed and validated an image translation framework for knee MRI sequences using CycleGAN. The enhanced images generated using our method allowed automatic and accurate segmentation of new knee MRI data without re-training. We expect this technique to lead towards fast and accurate quantification of large numbers of knee MRI which would result in improved and more targeted OA care.

ACKNOWLEDGMENT

BF is supported by an Alberta Innovates Graduate Student Scholarship for Data-Enabled Innovation. JJ is supported by the AHS Chair in Diagnostic Imaging. Academic time for JJ, RL and VQL is made available by Medical Imaging Consultants (MIC), Edmonton, Canada.

REFERENCES

[1] F. Eckstein *et al.*, "Quantitative mri measures of cartilage predict knee replacement: a case–control study from the osteoarthritis initiative," *Annals of the Rheumatic Diseases*, vol. 72, no. 5, pp. 707–714, 2013. [Online]. Available: https://ard.bmj.com/content/72/5/707

[2] E. Yamabe *et al.*, "Study of surgical indication for knee arthroplasty by cartilage analysis in three compartments using data from oai," *BMC musculoskeletal disorders*, vol. 14, no. 1, pp. 1–7, 2013.

[3] F. Eckstein *et al.*, "Magnitude and regional distribution of cartilage loss associated with grades of joint space narrowing in radiographic osteoarthritis–data from the osteoarthritis initiative (oai)," *Osteoarthritis and cartilage*, vol. 18, no. 6, pp. 760–768, 2010.

[4] M. Faschingbauer *et al.*, "Cartilage survival of the knee strongly depends on malalignment: a survival analysis from the osteoarthritis initiative (oai)," *Knee Surgery, Sports Traumatology, Arthroscopy*, vol. 28, no. 5, pp. 1346–1355, 2020.

[5] B. Norman, V. Pedoia, and S. Majumdar, "Use of 2d u-net convolutional neural networks for automated cartilage and meniscus segmentation of knee mr imaging data to determine relaxometry and morphometry," *Radiology*, vol. 288, no. 1, pp. 177–185, 2018.

[6] V. Couteaux *et al.*, "Automatic knee meniscus tear detection and orientation classification with mask-rcnn," *Diagnostic and interventional imaging*, vol. 100, no. 4, pp. 235–242, 2019.

[7] A. Tack, A. Mukhopadhyay, and S. Zachow, "Knee menisci segmentation using convolutional neural networks: data from the oai," *Osteoarthritis and cartilage*, vol. 26, no. 5, pp. 680–688, 2018.

[8] A. Tack and S. Zachow, "Accurate automated volumetry of cartilage of the knee using convolutional neural networks: data from the oai," in *2019 IEEE 16th International Symposium on Biomedical Imaging (ISBI 2019)*. IEEE, 2019, pp. 40–43.

[9] B. Felfeliyan *et al.*, "Toward accurate mri bone and cartilage segmentation in small data sets via an improved mask rcnn: data from the osteoarthritis initiative," *Osteoarthritis and Cartilage*, vol. 29, pp. S349–S350, 2021.

[10] J. L. Jaremko *et al.*, "Volumetric quantitative measurement of hip effusions by manual versus automated artificial intelligence techniques: An omeract preliminary validation study," in *Seminars in Arthritis and Rheumatism*. Elsevier, 2021.

[11] P. Khandelwal and P. Yushkevich, "Domain generalizer: A few-shot meta learning framework for domain generalization in medical imaging," in *Domain Adaptation and Representation Transfer, and Distributed and Collaborative Learning*. Springer, 2020, pp. 73–84.

[12] J. Harms *et al.*, "Paired cycle-gan-based image correction for quantitative cone-beam computed tomography," *Medical physics*, vol. 46, no. 9, pp. 3998–4009, 2019.

[13] S. Masoudi *et al.*, "Adipose tissue segmentation in unlabeled abdomen mri using cross modality domain adaptation," in *2020 42nd Annual International Conference of the IEEE Engineering in Medicine & Biology Society (EMBC)*. IEEE, 2020, pp. 1624–1628.

[14] E. Chiou *et al.*, "Harnessing uncertainty in domain adaptation for mri prostate lesion segmentation," in *International Conference on Medical Image Computing and Computer-Assisted Intervention*. Springer, 2020, pp. 510–520.

[15] K. Bousmalis *et al.*, "Unsupervised pixel-level domain adaptation with generative adversarial networks," in *Proceedings of the IEEE conference on computer vision and pattern recognition*, 2017, pp. 3722–3731.

[16] J.-Y. Zhu, T. Park, P. Isola, and A. A. Efros, "Unpaired image-to-image translation using cycle-consistent adversarial networks," in *Proceedings of the IEEE international conference on computer vision*, 2017, pp. 2223–2232.

[17] T. M. Quan, T. Nguyen-Duc, and W.-K. Jeong, "Compressed sensing mri reconstruction using a generative adversarial network with a cyclic loss," *IEEE transactions on medical imaging*, vol. 37, no. 6, pp. 1488–1497, 2018.

[18] B. Felfeliyan *et al.*, "Improved-mask r-cnn: Towards an accurate generic msk mri instance segmentation platform (data from the osteoarthritis initiative)," *arXiv preprint arXiv:2107.12889*, 2021.

[19] K. He, G. Gkioxari, P. Dollár, and R. Girshick, "Mask r-cnn," in *Proceedings of the IEEE international conference on computer vision*, 2017, pp. 2961–2969.

[20] C. G. Peterfy, E. Schneider, and M. Nevitt, "The osteoarthritis initiative: report on the design rationale for the magnetic resonance imaging protocol for the knee," *Osteoarthritis and cartilage*, vol. 16, no. 12, pp. 1433–1441, 2008.

[21] F. Ambellan, A. Tack, M. Ehlke, and S. Zachow, "Automated segmentation of knee bone and cartilage combining statistical shape knowledge and convolutional neural networks: Data from the osteoarthritis initiative," *Medical image analysis*, vol. 52, pp. 109–118, 2019.